Short Circuit Fault Localization Method Based on Improved OLS-RBF Neural Network Algorithm for AC Microgrids

Yibiao Huang
State Grid Fuzhou Electric Power Supply Company
Fuzhou, China
huangyibiao@126.com

Longyang Zhu
State Grid Fuzhou Electric Power Supply Company
Fuzhou, China
2239042194@qq.com

Yifan Wang
State Grid Fuzhou Electric Power Supply Company
Fuzhou, China
wyf688642@163.com

Hang Cheng
Fujian Rongneng Electric Power Group
Fuzhou, China
ch_7508@163.com

Yunting Shao
State Grid Fuzhou Electric Power Supply Company
Fuzhou, China
790034965@qq.com

Xin Zheng
College of Electrical Engineering and Automotion
Fuzhou University
Fuzhou, China
27480389@qq.com

2024 3rd Asia Power and Electrical Technology Conference (APET) | 979-8-3503-6769-0/24/$31.00 ©2024 IEEE | DOI: 10.1109/APET63768.2024.10882772

Abstract—**In order to improve the accuracy of short-circuit fault location in microgrids, this paper proposed a short-circuit fault location method for AC microgrids based on the improved OLS-RBF neural network algorithm. On the basis of amplifying microgrid short-circuit fault current signal using wavelet energy spectrum algorithm, the relationship between short-circuit current wavelet energy spectrum value and fault distance is investigated, and based on the European standard 400V low-voltage microgrid model, a coupling formula for fault location is constructed. Thus, a common fault area location model is established for both grid-connected and islanded modes. In the simulation experiments, the effect of transition resistance is taken into account to verify the accuracy of the method under different topological models.**

Keywords— microgrid, short circuit fault, neural network, fault location.

I. INTRODUCTION

As nonrenewable energy sources deplete and traditional energy generation burdens the environment, China urgently needs to adopt a new technological and industrial revolution to replace its previous development model with a more scientific and sustainable one. This has led to the emergence of the smart grid concept [1]. Wind and photovoltaic power, as representatives of distributed energy, are promoted for their environmental benefits, integrating into traditional power distribution systems as microgrids and transforming their structure. However, microgrids experience rapid inrush current during faults, complicating data protection and affecting AC protection accuracy. Thus, accurately diagnosing and locating faults during short circuits is a key research area in microgrids.

Recent studies on microgrid fault diagnosis have highlighted the integration of digital signal processing and neural networks. Literature [2] combines wavelet singular entropy with a self-organizing feature mapping neural network for accurate classification of changes in microgrid systems within one sampling period. However, its adaptability is limited and the model training process is complex. Literature [3] uses a great overlap discrete wavelet transform and back propagation neural network to quickly and accurately identify fault types, considering initial phase angle and transition resistances, but does not detail fault location. Literature [4] proposed a microgrid fault location method based on ARM model, which has a high quality of single-target fault location and little geographic coordinate error. However, it needs the signal support of the communication network, and visualization elements in the nonnetworked state are relatively few in number with a large deviation value. Literature [5] utilizes high-scale wavelet energy spectrum decomposition with the OLS-RBF neural network for early detection and regional location of short-circuit faults in microgrids. However, insufficient sampling capacity may lead to overfitting. Moreover, OLS-RBF neural networks are not universal and require frequent parameter adjustments due to changes in the training set, which leads to a complicated training process.

The proposed method in this paper is based on the literature [5] , and then improves the OLS-RBF neural network algorithm by introducing the gradient descent operator, so that each centroid has an independent centroid width. This improves the generalization performance of the algorithm. The model tuning process is simplified to adapt the neural network model to microgrid models with different topologies on the basis of ensuring the rapidity and accuracy of fault localization.

II. MICROGRID SHORT CIRCUIT FAULT ANALYSIS

A. Modeling of 400V Low Voltage Microgrids

Referring to the European 400V standard low-voltage microgrid structure [6], a simulation model is established by MATLAB/SIMULINK, as shown in Fig. 1. The distributed power in the model consists of energy storage battery, photovoltaic battery, and wind turbine, in which the energy storage battery is VF controlled and the rest of the distributed

power is PQ controlled. The power factors of the loads are all 0.85, the operating frequency of the microgrid model is 50 Hz, and the total length of the line is 600m.

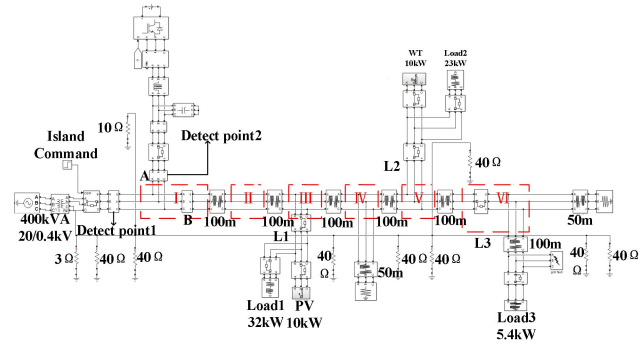

Fig. 1. Topology of 400V standard LV microgrid in Europe

B. Failure Analysis

The wavelet energy spectrum transform is a mathematical tool based on the Fourier transform, capable of effectively identifying and extracting subtle features within signals. At the same time, the multi-scale wavelet decomposition algorithm itself functions as a digital filter, efficiently suppressing noise interference in low-voltage systems [7]. In this paper, the derivative of the cubic B-spline function is chosen as the wavelet function, according to Mallat's algorithm [8], the wavelet energy spectrum transform equation for the discrete signal f(x) in the time domain is shown in (1).

In Equation(1), i represents the scale of wavelet decomposition, $S_{2^i}f(x)$ and $W_{2^i}f(x)$ are the smooth component and detail component at the i-th scale of wavelet decomposition, respectively, and $E_{2^i}f(x)$ is the energy of the details at the i-th scale. As i increases, the singularity of the fault signal is enhanced. However, as i increases, the computation speed decreases. Taking all factors into account, this paper selects the wavelet decomposition transform at the fourth scale. The impulse response coefficients of the low-pass filter h_k and the band-pass filter g_k are provided in Table I.

Based on Table I and Equation (1), the equations can be derived, where Equations (2) and (3) represent the smooth component at the third scale and the detail component at the fourth scale, respectively, and Equation (4) is the mathematical model of the wavelet energy spectrum used in this paper.

The wavelet energy spectrum algorithm is modeled in Simulink using existing components, as shown in Figure 2.

Wavelet transform can effectively extract local signal features, and the wavelet energy spectrum is based on the binary wavelet transform, which squares and amplifies the detailed components of the signal to improve the recognition of abrupt features of weak signals. In this paper, the first peak value of the wavelet energy spectrum, $E4_{max1}$, is obtained after a short-circuit fault occurs in AC microgrid by using wavelet energy spectrum algorithm, which amplifies the fault current signal during the short-circuit fault. Then, the relationship between $E4_{max1}$ and the fault distance d is analyzed.

$$\begin{cases} S_{2^i}f(x)=\sum_k h_k S_{2^{i-1}}f(x-2^{i-1}k) \\ W_{2^i}f(x)=\sum_k g_k S_{2^{i-1}}f(x-2^{i-1}k) \\ E_{2^i}f(x)=\left|W_{2^i}f(x)\right|^2 \end{cases} \quad (1)$$

TABLE I. THE COEFFICIENTS h_k AND g_k

k	- 1	0	1	2
h_k	0.125	0.375	0.375	0.125
g_k	0	-2	2	0

$$\begin{aligned} S_{2^1}f(n)&=\frac{1}{8}S_{2^0}f(n+1)+\frac{3}{8}S_{2^0}f(n)+\frac{3}{8}S_{2^0}f(n-1)+\frac{1}{8}S_{2^0}f(n-2) \\ S_{2^2}f(n)&=\frac{1}{8}S_{2^1}f(n+2)+\frac{3}{8}S_{2^1}f(n)+\frac{3}{8}S_{2^1}f(n-2)+\frac{1}{8}S_{2^1}f(n-4) \\ S_{2^3}f(n)&=\frac{1}{8}S_{2^2}f(n+4)+\frac{3}{8}S_{2^2}f(n)+\frac{3}{8}S_{2^2}f(n-4)+\frac{1}{8}S_{2^2}f(n-8) \end{aligned} \quad (2)$$

$$W_{2^4}f(n)=2(S_{2^3}f(n-8)-S_{2^3}f(n)) \quad (3)$$

$$E_{2^4}f(x)=\left|W_{2^4}f(x)\right|^2 \quad (4)$$

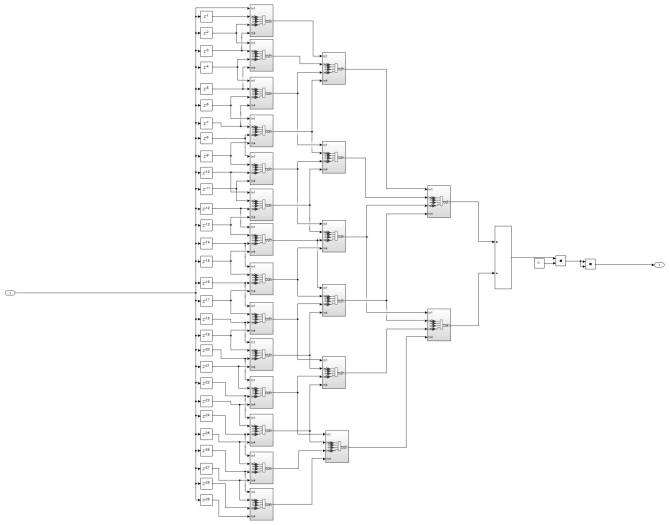

Fig. 2. The model of the wavelet energy spectrum algorithm

Previous research has shown that [9] when the distance d from the short-circuit fault point to the detection point increases, $E4_{max1}$ will decrease. Considering the actual value of $E4_{max1}$ is relatively large, we define the parameter $E4_{max1}=K_e/E4_{max1}$ where K_e takes the value of 10^6. Fig. 3 shows the relationship between d and $E4_{max1}$ for single-phase grounded short circuits under different values of θ_c.

As we can see from Fig. 3, $E4'_{max1}$ increases with the increase of d for different θ_c. After the simulation study, it is found that the conclusion is always consistent with the above for different capacity cases, different transition resistor resistance values and different short-circuit fault types [10]. Therefore, considering different factors, the value of the fault current measured at the detection point can approximately reflect the distance d from the short-circuit fault point to the detection point, thus realizing the regional localization of the short-circuit fault.

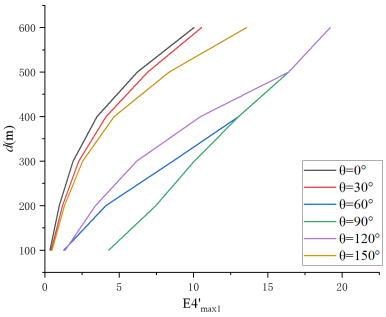

Fig. 3. Relationship between *d* and *E4'max1* for different *θc*

III. FAULT LOCATION ANALYSIS BASED ON NEURAL NETWORK

A. Principle of OLS-RBF Neural Network Algorithm

As shown in Fig. 4, the radial basis function neural network consists of three layers of neurons: the input layer, the hidden layer and the output layer, which theoretically has the ability to approximate any nonlinear function. Among them, the input layer receives training data, the sample capacity is n; the implicit layer transforms the low-dimensional linearly indivisible problem of the input layer into a high-dimensional space with the help of a radial basis function so as to realize a linearly differentiable. The radial basis function is usually selected Gaussian function, the mapping relationship as shown in (5). As the sample point is closer to the center point, the implicit layer output is higher. The output layer is connected to the implicit layer by linear weights, as shown in (6). In Equation (6), y represents the actual value, and $\hat{y}$ represents the predicted value. From (5) and (6), the radial basis function center point c_i , width σ_i and output weights λ_i affect the accuracy of the neural network model together.

The OLS-RBF neural network selects the center points of the radial basis function by orthogonal least squares, and determines the contribution of each sampling point to the reduction of the output error, so as to minimize the overall error until it meets the set requirements. Compared with the K-means clustering method, the OLS-RBF neural network does not need to preset the center points, and the order of contribution is fixed when the sampling points are determined, i.e., the accuracy of the model is only related to the number of center points in the hidden layer. The flow of the algorithm is shown in Fig. 5 [11].

After the above process, a radial basis function neural network model based on orthogonal least squares can finally be obtained. It can be found that when the sampling points and their corresponding truth values are unchanged, the center point selection is unchanged, and there are no random events in the model construction process. However, if the capacity of the sampling points is small, it may lead to all the sampling points being selected as the center point, overfitting occurs, and the expected fitting accuracy cannot be achieved. In addition, the OLS-RBF neural network is not universal, and whenever the training set is changed, the width of the center point in the program needs to be constantly modified, and the training process is more complicated.

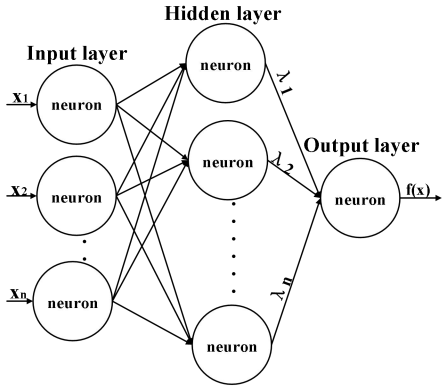

Fig. 4. Schematic diagram of RBF neural network

$$\phi\left(\left\|x-c_i\right\|\right)=\exp\left(-\frac{\left\|x-c_i\right\|}{2\sigma_i^2}\right) \tag{5}$$

$$y=\hat{y}+\varepsilon=\sum_{i=1}^{n}\lambda_i\phi_i\left(\left\|x-c_i\right\|\right)+\varepsilon \tag{6}$$

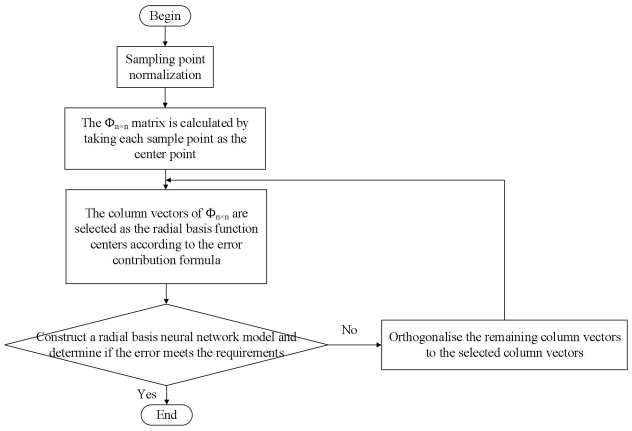

Fig. 5. Flowchart of OLS-RBF neural network model

B. Improved OLS-RBF Neural Network Algorithm

In order to reduce the number of neurons in the hidden layer of the OLS-RBF neural network and to improve the generalization ability of the algorithm, a gradient descent operator is introduced into the original OLS-RBF neural network so that each centroid has an independent centroid width σ_i . The structure of the improved OLS-RBF neural network algorithm is shown in Fig. 6.

The principle of the gradient descent operator is as follows: each radial basis function center point initially has a width value σ . To optimize the model, the width of each center point needs to be adjusted to minimize the output error. First, the root mean square error (rmse) under the current conditions is calculated using Equation (7), representing the error between the model output and the true value. The goal of the gradient descent method is to gradually adjust the center point width σ to reduce this error.

The gradient descent method uses the gradient of the error to adjust the width. The update equation for the center point width is shown in Equation (8). In Equation (8), σ^* is the updated width, and ω is the learning rate. This value can be

set relatively large in the initial phase of the program to widen the search range for σ. When the difference between σ^* and σ becomes small, the learning rate should be reduced to a very small value. $\triangle\sigma$ is the change in the center point width, and its calculation equation is shown in Equation (9).

If $\triangle\sigma > 0$, it indicates that the current adjustment direction of the width σ helps reduce the error, and the adjustment should continue in the current direction to approach the optimal value. If the gradient change is small, it indicates that the width adjustment is stabilizing, and the learning rate ω should be reduced to more precisely find the minimum error.

When the difference in the error becomes sufficiently small or the maximum number of iterations is reached, the gradient descent process ends, and the optimal width value for each basis function is obtained.[11]

For a single-phase grounded short-circuit fault, set the range of DG capacity of the built simulation model as 10-60kW, with sample points at $S_{DG} \in \{10, 20, 30, 40, 50, 60\}$.Due to the symmetry of the fault occurrence, only half a cycle need to be analyzed, with initial phase angles $\theta_c \in \{0, 30, 60, 90, 120, 150\}$ The short-circuit point transition resistance is $R_g \in \{0.01, 0.05, 0.1, 0.5, 1\}$, and the fault distance is set as $d \in \{100, 200, 300, 400, 500, 600\}$. This results in a total of 1,080 data sets, with 80% used for training and 20% for testing. Figure 7 illustrates the modeling process of various neural networks for the objective function d, showing that the improved OLS-RBF neural network requires fewer implicit layers to converge and takes less time during debugging.

The trained radial basis function centroid c_i, output weights λ_i and centroid width σ_i are substituted into (6) to obtain the functional relationship between the fault distance d and S_{DG} ,θ_c , R_g, $E4'_{max1}$ as in (10). Fig. 8 shows the prediction accuracy of the two neural network models for the test set in the grid-connected, where the pre-improved R^2 is 97.56% and the improved R^2 can reach 98.99%.

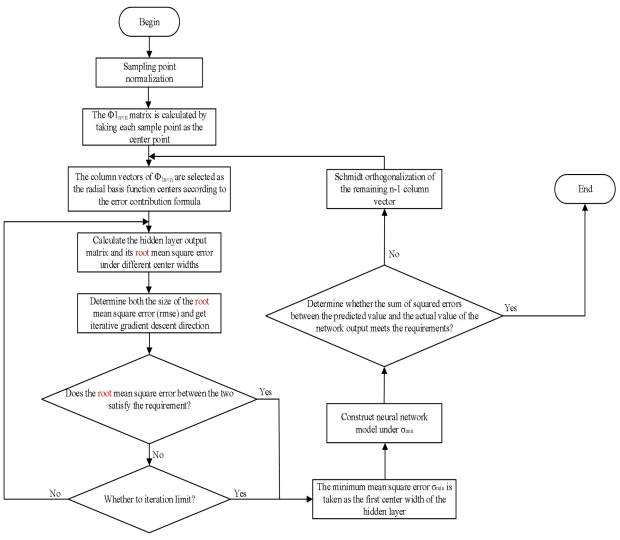

Fig. 6. Flowchart of OLS-RBF neural network model

$$\delta_{RMSE} = \sqrt{\|y - \phi_n \lambda\|^2 / n} \tag{7}$$

$$\sigma^* = \sigma - \omega \triangle\sigma \tag{8}$$

$$\triangle\sigma = (\delta_{RMSE1} - \delta_{RMSE2}) / (\sigma^* - \sigma) \tag{9}$$

$$d = \sum_{i=1}^{864} \lambda_i \exp\left(- \frac{\sqrt{(S_{DG} - c_i)^2 + (\theta_c - c_i)^2 + (E4'_{\max 1} - c_i)^2 + (R_g - c_i)^2}}{2\sigma_i^2} \right) \tag{10}$$

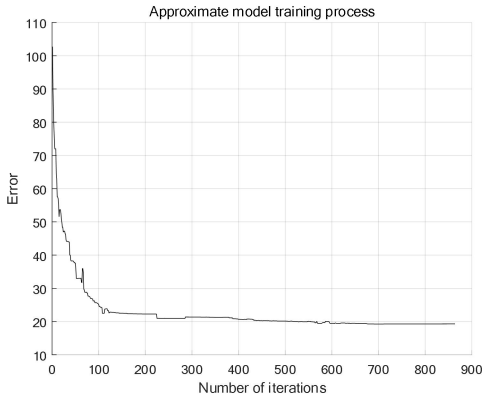

(a) OLS-RBF neural network

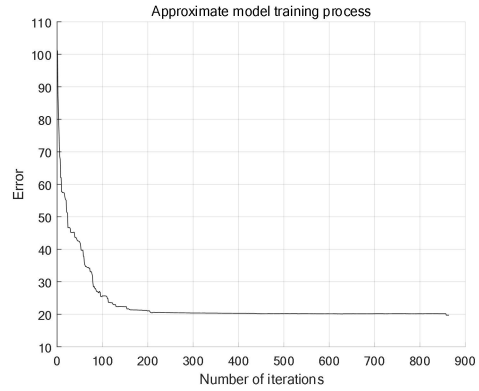

(b) Improved OLS-RBF neural network

Fig. 7. Approximate modeling process of different neural networks for the objective function d

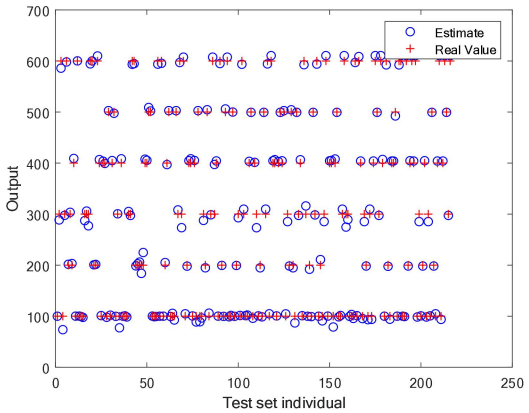

(a) OLS-RBF neural network

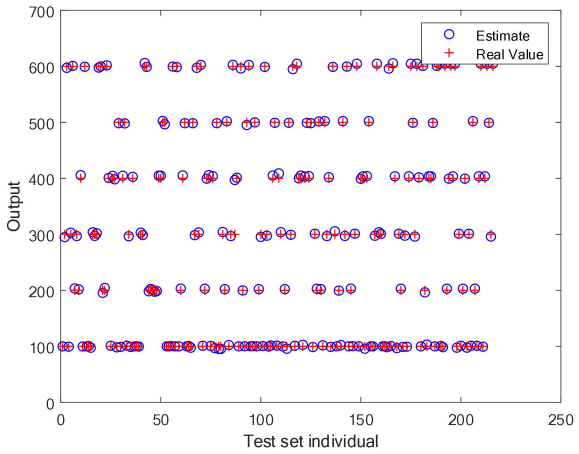

(b) Improved OLS-RBF neural network

Fig. 8. Fault location prediction accuracy map in grid-connected operation mode

IV. Simulation Verification

A. Initial Phase Angle of Fault θ_c Determination and Short Circuit Fault Type Identification

From Fig. 3 and (10), it can be seen that it is necessary to determine the initial phase angle θ_c of the fault and determine the fault type before fault region localization by $E4'_{max1}$. When $E4$ reaches the detection threshold X_d, the system gets the preliminary fault initial phase angle detection value θ and the calculation formula is shown in (11).

$$\theta = K_j \times S_t \times 10^{-4} \times 180^{\circ} \tag{11}$$

where S_t denotes the simulation step size in Simulink, which is set to 50us in this paper according to the accuracy requirement; K_j is the number of times the fault initial phase angle detection module runs. Since the wavelet energy spectrum characteristics are the same when the fault occurs in the positive and negative half-waves, this parameter is reset when the current is at the point of crossing the zero point. As there is an interval Δt between the detection of the fault occurrence and the actual occurrence of the fault, the detection value θ needs to be processed as shown in Equation (12) to obtain a more accurate initial phase angle of the fault θ_c. Figure 9 shows the detection model of the initial phase angle of the fault θ_c.

$$\theta_c = \theta - \Delta\theta \tag{12}$$

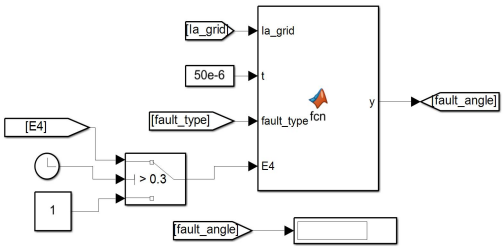

Fig. 9. Initial phase angle of fault θ_c Detection model

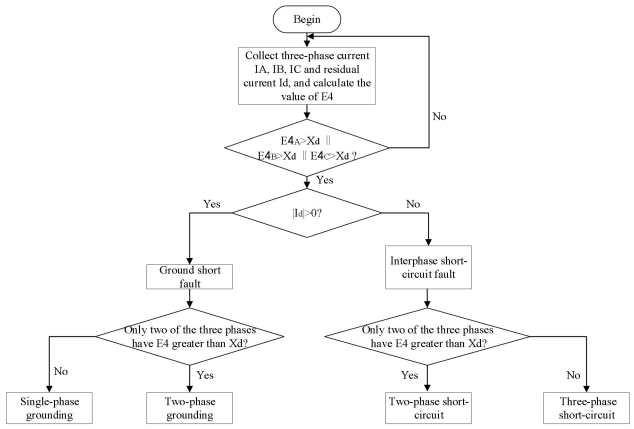

Fig. 10. Block diagram of short-circuit fault type judgment program

Figure 10 shows the short circuit fault type judgment process. Since the microgrid model established in this paper is a three-phase four wire system, the residual current can be used to determine whether the short circuit fault is grounded, and then the faulted phases and the fault type can be determined based on whether the $E4$ values of the currents in each of the phases of $\dot{I}_a$, $\dot{I}_b$, and $\dot{I}_c$ exceed the threshold values.

B. Simulation Modeling

According to the above analysis of the principle of fault area localization, design the area localization simulation model, as shown in Fig. 11. The realization steps are as follows:

1) Based on the early detection thresholds X_d set earlier, when the measured $E4$ value is greater than X_d, the fault is judged to have occurred;

2)Determine whether current is passing through the grid-connected point;

3) Detect the initial phase angle of the fault θ_c;

4) Identify the type of fault;

5) Detect the maximum $E4$ value within 1ms as $E4_{max1}$ and calculate $E4'_{max1}$;

6) Calculate the fault distance d by substituting the initial fault phase angle θ_c, $E4'_{max1}$, and the S_{DG} and R_g set by the system into the fault area location equation for the fault type, then determine the fault area.

C. Simulation results and analysis

The simulation verification data for different short-circuit fault types are shown in Table II, where t_1 denotes the early detection time, and t_2 denotes the total time from early detection to fault location for short-circuit faults. From the data in the table, it can be seen that the protection system is able to realize the early detection of the fault within 1ms, and accurately identify the fault type and complete the fault location within 2ms.The fault settings are distributed across six regions in Figure 1, and the measurement results are consistent with the area where the fault point is located.

The proposed method has been compared with the traveling wave distance measurement method from literature [12] at different fault distances and the results are listed in Table III. It can be seen from the table that the method proposed in this

paper has a significant advantage in terms of positioning accuracy.

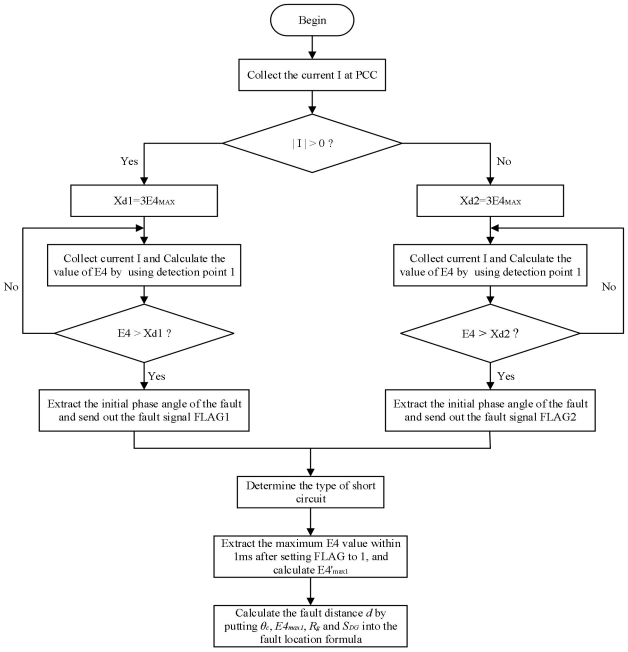

Fig. 11. Protection system operation flow

V. CONCLUSION

In summary, this paper proposes a fault location method which is based on improved OLS-RBF neural network algorithm on the ground of using wavelet energy spectrum algorithm to amplify the fault current, while satisfying the requirements of quickness and accuracy of fault area location, it reduces the complexity of the network model, simplifies the model training process, and enhances the generalizability of the proposed method. In addition, a generalized fault area localization model is established for both grid-connected and islanded modes.

TABLE II. SHORT-CIRCUIT FAULT PROTECTION SIMULATION VERIFICATION RESULTS

Type &. Distance of fault (*d*/m)	running mode	S_{DG}(KW)	θ_c(°)	t_1	t_2	*Localization results of fault area*
AG (268)	*isolated island*	*43*	*136*	*0.363*	*1.384*	Region III
AG (427)	*grid connection*	*41*	*177*	*0.490*	*1.523*	Region V
AG (508)	*grid connection*	*38*	*131*	*0.362*	*1.387*	Region VI
AG (63)	*isolated island*	*42*	*173*	*0.453*	*1.574*	Region I
ABG (589)	*grid connection*	*26*	*105*	*0.268*	*1.620*	Region VI
ABG (212)	*isolated island*	*39*	*50*	*0.336*	*1.650*	Region III
ABG (109)	*isolated island*	*10*	*4*	*0.465*	*1.718*	Region II
ABG (336)	*grid connection*	*28*	*121*	*0.441*	*1.469*	Region IV
AB (498)	*isolated island*	*37*	*81*	*0.269*	*1.792*	Region V
AB (560)	*grid connection*	*59*	*76*	*0.563*	*1.887*	Region VI
AB (446)	*isolated island*	*12*	*151*	*0.245*	*1.597*	Region V
ABC (600)	*isolated island*	*55*	*139*	*0.562*	*1.704*	Region VI
ABC (358)	*grid connection*	*17*	*66*	*0.446*	*1.767*	Region IV

TABLE III. FAULT LOCATION PERFORMANCE COMPARISON OF DIFFERENT PROTECTION METHODS

fault localization method	fault distance (m)	localization result (m)	relative error (%)
the method described in this paper	*820*	*826*	*0.7*
	880	*889*	*1.0*
Traveling wave distance measurement method	*820*	*1040*	*26.8*
	880	*1040*	*18.2*

ACKNOWLEDGMENT

This work is financially supported by "Technology Project of State Grid Fujian Electric Power Co., Ltd." (No. 521310240008).

REFERENCES

[1] Zeng Ming, Yang Yongqi and Liu Dunnan ,et a1,″ Generation-Grid-Load-Storage" Coordinative Optimal Operation Mode of Energy Internet and Key Technologies ″ , *Power System Technology*,vol.40,no.1,pp.114-124, January 2016.

[2] Qiu Lu, Ye Yinzhong and Jiang Chundi, ″Fault diagnostic method for micro-grid based on wavelet singularity entropy and SOM neural network″, *Journal of Shandong University(Engineering Science)*, vol. 47, no. 5, pp. 118-122+129, October 2017.

[3] Chen Jiahui , Gao Yanjie , Jin Yiwei, ″ A New Microgrid Fault Diagnosis Method Based on MODWT and BP Neural Network ″ , *Journal of Shanghai University of Electric Power*,Vol.37,no.1,pp.57-60+77, February 2021.

[4] Zeng Yihui, Shu Yingjun, Mai Junjia, Li Bin, Wu Xinqiao, ″A Beidou Fault Location Method for AC Microgrids Based on Arm Model ″ , *Power System and Clean Energy*,Vol.39,no.4,pp.99-104,April,2023.

[5] Zheng Xin and Gan Honghao, ″Early Detection and Regional Location of Short Circuit Fault for Grid-connected AC Microgrid with Different Capacity″, *Proceedings of the CSEE*,vol. 44, no. 11, pp. 4353-4367, 2024.Available: http://kns.cnki.net/kcms/detail/11.2107.tm.20230308.0921.012.html.

[6] PAPATHANASSIOU S, HATZIARGYRIOU N, STRUNZ K, ″ A benchmark low voltage microgrid network ″, Proceedings of CIGRE Symposium: *Power Systems with Dispersed Generation*, Athens, Greece, pp. 1-8, April 2005.

[7] Chen Li'an and Zhang Peiming, "Early Detection of Short Circuit Faults in Low Voltage Systems Based on Morphological Wavelets," *China Electric Power Research Institute*, vol. 10, no. 1, pp. 24-28+88, May 2005.

[8] S. Mallat and S. Zhong, "Characterization of signals from multiscale edges," *IEEE Transactions on Pattern Analysis and Machine Intelligence*, vol. 14, no. 7, pp. 710-732, July 1992.

[9] Zeng Yue,″Design and Implementation of Short-Circuit Fault Protection System in Grid-Connected AC Microgrid ″,Fuzhou University,April 2022.

[10] Zhou Yanfang, Wang Ying, Huang Tao, Mao Weijun and Hu Zhesheng, ″ Research on influence of transition resistance on microgrid fault detection″, *Modern Electronics Technique*, vol. 45, no. 17, pp. 157-162, September 2022.

[11] Zhao Fumin, ″ Research on multi-objective optimization method of electromagnetic actuator with permanent magnet ″ , Fuzhou University,April 2022.

[12] Dai Feng, Wang Zheng, Cheng Menghan, et al., "Study on fault location considering refraction and reflection of short lines in a distribution network," *Power System Protection and Control*, vol. 48, no. 16, pp. 122-130, 2020.